

Orders-of-magnitude reduction in photonic mode volume by nano-sculpting

Rasmus E. Christiansen^{1,3,*}, Jesper Mørk^{2,3}, and Ole Sigmund^{1,3}

¹*Department of Civil and Mechanical Engineering, Technical University of Denmark, Nils Koppels Allé 404, DK-2800 Kgs. Lyngby, Denmark*

²*Department of Electrical and Photonics Engineering, Technical University of Denmark, Ørsteds Plads 343, DK-2800 Kgs. Lyngby, Denmark and*

³*NanoPhoton - Center for Nanophotonics, Technical University of Denmark, Ørsteds Plads 345A, DK-2800 Kgs. Lyngby, Denmark.*

Three-dimensionally sculpted dielectric nanostructures supporting material(air) confined optical modes with single-emitter mode volumes three(four) orders of magnitude below the diffraction limit, $V_{\mathbf{r}_0} \approx 0.0004 [\lambda/(2n)]^3$ ($V_{\mathbf{r}_0} \approx 0.00003 [\lambda/2]^3$), are discovered using topology optimization. Encapsulating the nanostructure by ellipsoidal shells enables seemingly unbounded mode quality factor enhancement ($Q > 10^8$ demonstrated numerically) leading to Purcell enhancement above 10^{11} . It is studied how $V_{\mathbf{r}_0}$ and Q depend on the choice of material, device volume, minimum feature size and number of shells.

For a single emitter (atom) situated at a point \mathbf{r}_0 in space the Purcell enhancement of its interaction with the electromagnetic field (the light-matter interaction), is proportional to the ratio between the spectral and spatial confinement of the light at \mathbf{r}_0 , i.e. $F \propto \frac{Q}{V_{\mathbf{r}_0}}$ [1]. Here, Q denotes the quality factor and $V_{\mathbf{r}_0}$ the single-emitter mode volume associated with the electromagnetic resonance of the environment surrounding the emitter. Several potentially ground-breaking applications depend on achieving strong light-matter interaction [2], e.g. realizing efficient single-photon sources for quantum technology [3] or nano-scale lasers and light-emitting diodes [4–6]. While some applications can rely on large Q -values to achieve sufficient interaction strength, many applications (like optical switches) require high operating speeds and thus large optical bandwidths; are footprint-constrained or are otherwise spectrally limited, bounding Q from above. Such applications must instead exploit strong spatial confinement of the field, i.e. small mode volumes, to increase F . Extreme spatial confinement may be achieved using plasmonic structures, at the unavoidable cost of significant energy loss to heating and limited spectral confinement ($Q < 100$) [7]; both being unacceptable conditions for many applications.

Achieving $V_{\mathbf{r}_0} < 1 [\frac{\lambda}{2n}]^3$ in dielectric structures was long deemed unattainable, but recent works have demonstrated this to be possible through so-called Extreme Dielectric Confinement (EDC) both numerically and experimentally [8–15] in platforms made of silicon $V_{\mathbf{r}_0} \approx 0.08 [\lambda/(2n_{\text{Si}})]^3$ [16], and indium phosphide, $V_{\mathbf{r}_0} \approx 0.26 [\lambda/(2n_{\text{InP}})]^3$ [17]. These achievements have opened a new avenue for enhancing light-matter interaction in near-lossless dielectric environments capable of supporting high Q -values.

Until now, exploration of the EDC phenomenon has been restricted to two-dimensionally (2D) patterned planar devices relying on few-nanometer-sized geometric features to facilitate strong in-plane field confinement (Fig. 1a). As state-of-the-art nanofabrication capable of realizing features at the few-nanometer scale is limited to patterning 2D-layers of material [18], such a restriction is sensible. However, considering technological advances in three-dimensional (3D) nanoscale fabrication, where the 3D-printing of structures with features in the hundred nanometer range is approaching routine [19, 20], realizing 3D-sculpted geometries with features at the few-nanometer scale may become feasible in the near future. Possibly using technologies based on implosion fabrication [21], ice-lithography [22] or focused ion-beam milling [23] coupled with advanced nano-assembly technologies [24].

In this paper we demonstrate the possibility of realizing orders of magnitude improvement of the Q -over- V ratio by three-dimensional sculpting of the electromagnetic environment using inverse design by Topology Optimization (TopOpt) [25, 26], which has garnered significant interest for nanophotonic applications in recent years [27, 28]. First, a study of the full 3D design problem reveals a reduction in the achievable $V_{\mathbf{r}_0}$ with increasing 3D design freedom (Fig. 2). Then, by exploiting a fundamental symmetry discovered from the 3D-sculpted structures (Fig. 3) the problem is reduced to an axisymmetric sculpting problem enabling extreme design resolution, in turn allowing the discovery of a structure supporting an air-confined mode with $V_{\mathbf{r}_0} \approx 0.00003 [\lambda/2]^3$ (Fig. 1c) and another supporting a material-confined mode with $V_{\mathbf{r}_0} \approx 0.0008 [\lambda/(2n_{\text{Si}})]^3$ simultaneously allowing for extreme spectral confinement ($Q > 10^8$) by embedding the structure in ellipsoidal shells (Fig. 4). Finally, the effect of the dielectric material choice, device

* Corresponding email: raelch@dtu.dk

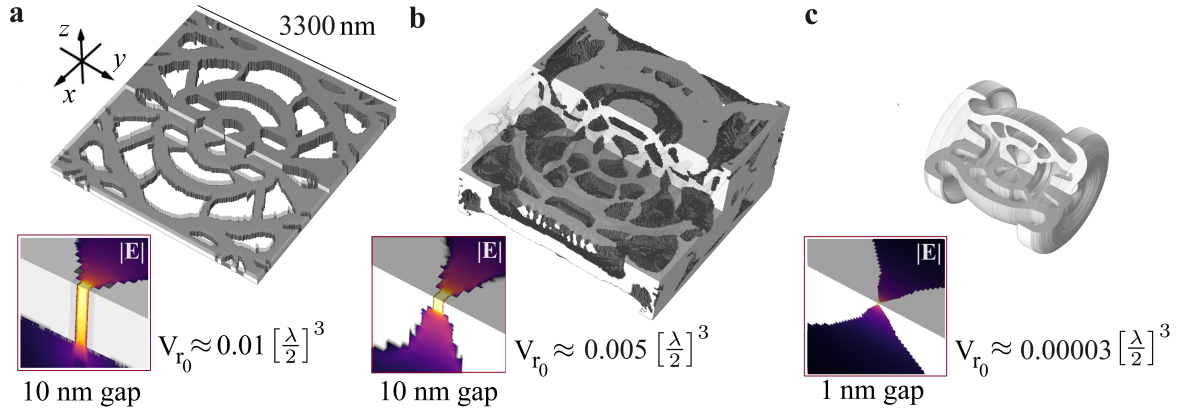


FIG. 1. **(a)** Planar 2D-patterned dielectric cavity (gray). **(b)** 3D-sculpted dielectric cavity. **(c)** Axisymmetric 3D-sculpted dielectric cavity. Each panel include a zoom of a quarter of the geometry centered at \mathbf{r}_0 showing the electric field magnitude (inferno) of the air-confined mode and lists the associated single-emitter mode volume.

volume and minimum feature-size on $V_{\mathbf{r}_0}$ is studied (Fig. 5), in the process finding a silicon structure with 1 nm solid bridge-feature at \mathbf{r}_0 exhibiting $V_{\mathbf{r}_0} \approx 0.0004 [\lambda / (2n_{\text{Si}})]^3 \approx 1.2 \cdot 10^{-6} [\lambda]^3$.

As the objective function to be minimized in our TopOpt-based sculpting process, we adopt an approximation of the single-emitter mode volume at \mathbf{r}_0 , which is rigorously defined using the theory of quasi-normal modes [29], computed under external planewave excitation,

$$\Phi = \frac{\int_{\Omega_I} \varepsilon_r(\mathbf{r}) |\mathbf{E}(\mathbf{r})|^2 d\mathbf{r}}{\varepsilon_r(\mathbf{r}_0) |\mathbf{E}(\mathbf{r}_0)|^2} \approx V_{\mathbf{r}_0}. \quad (1)$$

Here $\Omega_I \subset \mathbb{R}^3$ denotes the spatial domain being modelled, $\mathbf{E}(\mathbf{r})$ the time-harmonic electric field resulting from the external excitation and $\varepsilon_r(\mathbf{r})$ the spatially dependent relative permittivity. To simulate the electric field in Ω_I , we employ a classical electromagnetics model, assuming time-harmonic field behavior with one first order scattering boundary condition to truncate the modelling domain and another to introduce a Gaussian-enveloped ($\sigma = 500$ nm), linearly-polarized, planewave exciting the structure.

The initial study is carried out employing a fully three-dimensional model, while the subsequent studies are carried out using an efficient axisymmetric model assuming field invariance in the azimuthal direction $\mathbf{E}(r, \phi, z) = \mathbf{E}(r, z)$, i.e. only targeting the lowest order (constant) mode in the azimuthal expansion. The physics model problem is discretized and solved using the finite-element method (FEM) [30] and the inverse design problem is solved using the Method of Moving Asymptotes (MMA) [31], all implemented utilizing COMSOL Multiphysics [32].

The material distribution in Ω_I , constituting the

device under design, is controlled by a design field $\xi(\mathbf{r}) \in [0, 1]$, which is iteratively updated to minimize Φ subject to a length-scale constraint [33] controlling the smallest possible feature size of the structure. The design field is linked to the physics model by linearly interpolating the relative permittivity $\varepsilon_r(\mathbf{r})$ in Ω_I between a background material ($\xi(\mathbf{r}) = 0$) and the device material ($\xi(\mathbf{r}) = 1$) after subjecting the design field to a standard smoothing and thresholding procedure [34]. All structures are designed starting from a single uniform initial guess ($\xi(\mathbf{r}) = 0.5$). The facts that we select a fixed \mathbf{r}_0 as our reference point to compute $V_{\mathbf{r}_0}$ and enforce a minimum length scale of the optimized structures ensure that we do not rely on a lightning-rod type effect to create singularities in the electric field resulting in artificially small mode volumes [35].

First, we study the effect of introducing 3D-design freedom on the achievable $V_{\mathbf{r}_0}$ and the device geometry. To this end, a planar 2D-patterned membrane and a set of 3D-sculpted structures are inversely designed for air-confinement at \mathbf{r}_0 using a (computationally) limited but directly comparable design resolution with a minimum voxel size of 10 nm, assuming an air background ($n = 1.0$) and a device material corresponding to indium phosphide (InP) at $\lambda = 1550$ nm ($n = 3.17$). The resulting structures and corresponding mode volumes are presented in Fig. 2 (note that all mode volumes reported in this work are calculated by solving an eigenvalue problem using a high-resolution model to obtain the appropriate eigenmode for each optimized structure and not using the planewave excitation employed in the design process). As seen from Fig. 2, the mode volume decreases with increasing out-of-plane design freedom (device thickness). This reduction of $V_{\mathbf{r}_0}$ comes at the cost of a more complex geometry. The

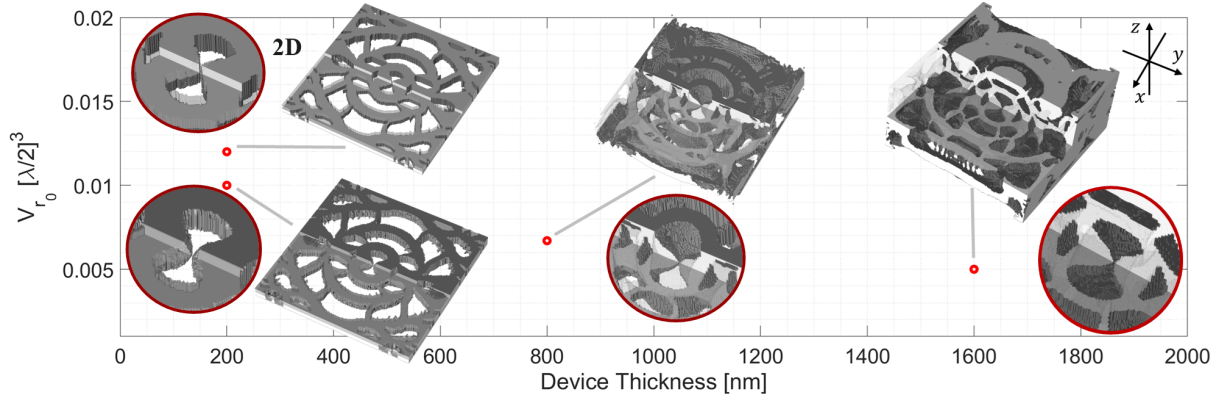


FIG. 2. Mode volume (V_{r_0}) for devices sculpted using the 3D model as a function of allowed device thickness, inserts show the optimized geometries with zooms of the regions surrounding r_0 for the indicated points.

single-emitter mode volume decreases by a factor of approximately 2 when increasing the device thickness from 200 nm to 1600 nm. This relatively limited reduction in V_{r_0} is a consequence of the limited model resolution possible when treating the full 3D problem numerically, as will become clear in the following studies. By comparing $|\mathbf{E}|$ shown in the zooms in Fig. 1a and Fig. 1b, it is directly observed that introducing 3D design freedom leads to tighter out-of-plane field confinement at r_0 .

Remarkably, when studying the 3D-sculpted structures in Fig. 2, a bowtie-like torus, and other near-axisymmetric features, are seen to develop in the region near r_0 as the design thickness increases (see the zoomed inserts), suggesting a fundamental symmetry of the optimal structure. To investigate this further, both the geometry and the field profile of the mode localized at r_0 is studied for the 1600 nm thick structure (see Fig. 3a-3b). Here we make a striking finding, namely that even though complete 3D-sculpting freedom was allowed in the inverse design process, both the optimized geometry and the resulting eigenmode electric-field profile exhibit near-axisymmetric behavior (around the y -axis) in the vicinity of r_0 .

Based on this observation, an axisymmetric model is employed to sculpt a structure with identical material and geometry parameters, resulting in the geometry shown in Fig. 3c. When comparing Fig. 3a and Fig. 3c similar geometric features and electric field profiles are observed. Utilizing this finding, the 3D physics model is replaced by the axisymmetric physics model, hereby enabling numerical studies at significantly finer geometric resolution and larger overall device sizes.

Employing the computationally-efficient axisymmetric model we first investigate the achievable single-emitter mode volume when confining the field in the air (Fig. 1c). Here a 1 nm air gap (minimum

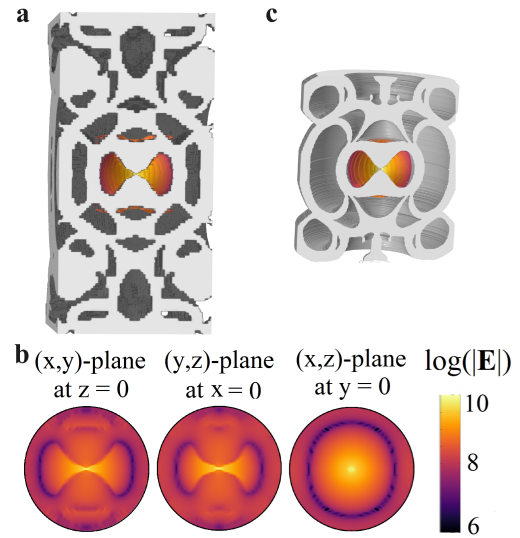


FIG. 3. (a) (y,z) -plane cut at $x=0$ of 3D-sculpted 1600 nm thick structure from Fig. 2. (b) Electric field magnitude in the (x,y) -, (y,z) - and (x,z) -planes through r_0 of targeted mode. (c) (y,z) -plane cut at $x=0$ through axisymmetric device geometry. (a) and (c) include overlays showing $\log_{10}(|\mathbf{E}|)$ for the targeted mode within a radius of 400 nm of r_0 .

feature size) is enforced at r_0 , comparable to what was recently experimentally demonstrated to be fabricable when considering planar 2D-patterned devices realized using self-assembled silicon (Si) nanostructures [24]. This structure is found to support a mode with $V_{r_0} \approx 0.00003 [\lambda/2]^3$. Thus it is revealed, that through 3D-sculpting it is possible to achieve single-emitter mode volumes nearly five orders of magnitude below the diffraction limit for field confinement in a 1 nm air gap (a more than 50x smaller V_{r_0} than what was reported theoretically for a planar nano-beam [11] with an identical gap size).

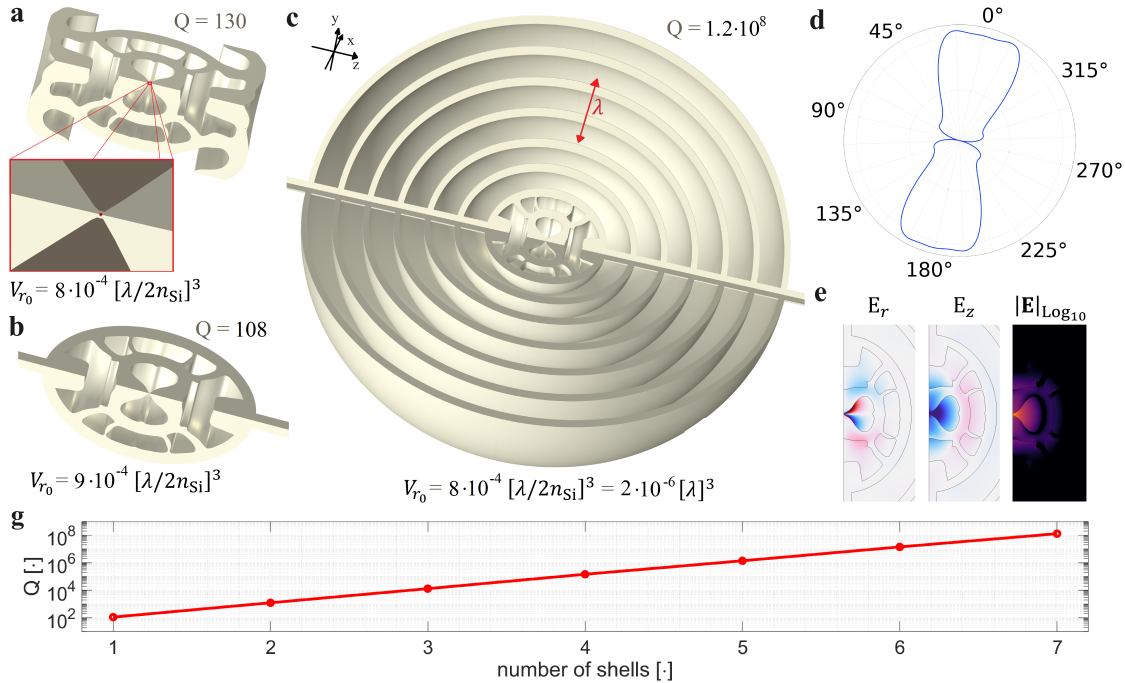


FIG. 4. Quarter revolution of (a) axisymmetric silicon device with a fixed 2 nm diameter central solid bridge-feature. (b) simplified geometry with ellipsoidal shell and connecting rod. (c) Three-quarter revolution of simplified geometry with six additional ellipsoidal shells. (d) Far-field emission pattern in the (x,z) -plane. (e) electric near-field components and magnitude. (g) Quality factor of the relevant mode Q as a function of the number of shells.

Next, employing the axisymmetric model we investigate the achievable single-emitter mode volume when confining the field in a solid bridge (cylinder). To this end, we assume a background index of $n = 1.0$ and a device material index of $n = 3.48$ (silicon at $\lambda = 1550$ nm) and enforce a fixed 2 nm diameter central solid bridge-feature. The inversely designed structure obtained under these conditions is presented in Fig. 4a.

This device supports a single-emitter mode volume of $V_{r_0} \approx 8 \cdot 10^{-4} [\lambda / (2n_{Si})]^3$ for the appropriate eigenmode, two orders of magnitude smaller than the mode volume reported in [16] for a 2D-patterned silicon structure. Observing that the electric near-field profile immediately outside the device geometry is approximately ellipsoidal, a simplification of the geometry is made by replacing the outermost part by an ellipsoidal shell, see Fig. 4b. This operation simplifies the geometry at the cost of increasing V_{r_0} by approximately 10%. In turn this simplification enables systematic control of the mode quality factor through the introduction of additional ellipsoidal shells with parameter-optimized radii and thicknesses. These shells are spatially disconnected from each other resulting in a mechanically infeasible structure. However, introducing a solid rod along the z -axis where it is observed that the emission pattern exhibits a node (Fig. 4d) connecting all shells

to each other and to the central device, has almost no effect on the obtainable Q . Figure 4c shows a rendering of the device with six shells and the rod added, raising the quality factor from $Q \approx 130$ to $Q \approx 1.2 \cdot 10^8$ without increasing V_{r_0} . The shells operate as a Bragg-like mirror, each layer increasing Q by approximately one order of magnitude as reported in Fig. 4f. Thus, if the emitter-cavity structure is limited by the linewidth of the cavity rather than homogeneous broadening of the emitter [36], the device shown in Fig. 4c supports a Purcell enhancement of $F \approx 10^{11}$, which is several orders of magnitude greater enhancement than what was observed for a previously proposed 2D-patterned nanobeam device [11] both due to significantly smaller V_{r_0} and larger Q . The far-field profile and the near-field of the device in Fig. 4c are visualized in Figs. 4d and 4e respectively.

Finally, the effects of the dielectric material (assuming an air background $n_{BG} = 1.0$); the maximum allowable device volume; and the minimum allowed feature size in the structure are studied in detail through three parameter studies (see Fig. 5). Here a total of fifteen axisymmetric devices are inversely designed for minimizing V_{r_0} .

In the first study, seven devices are sculpted to study the effect of the material refractive index. Here a central feature width of 8 nm and an overall de-

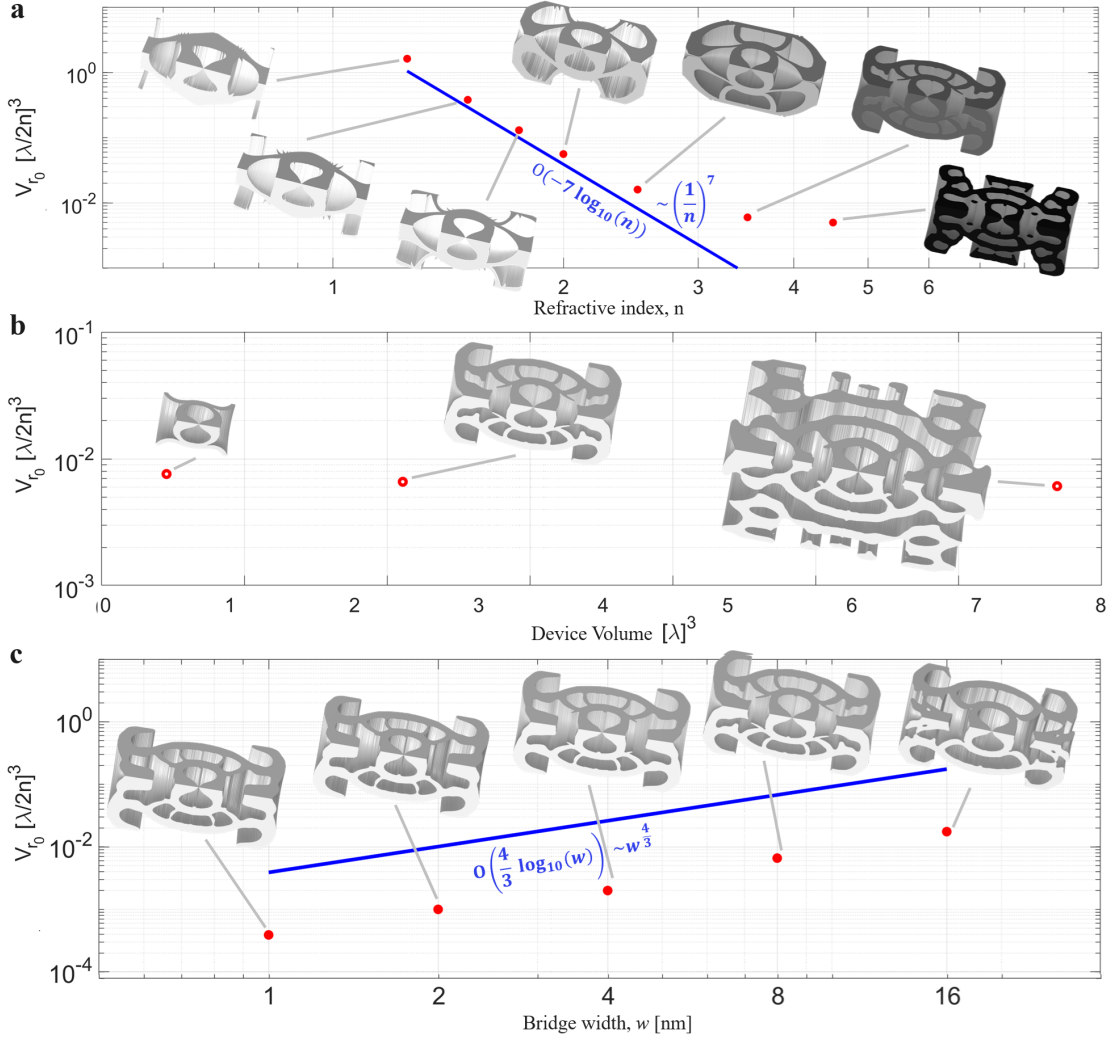


FIG. 5. V_{r0} for sets of sculpted structures as a function of the (a) refractive index, (b) device volume, (c) central bridge width. The inserts show a 90° revolution of the optimized axisymmetric geometries.

vice volume of approximately $2[\lambda]^3$ is used, see Fig. 5a. Remarkably, it is observed that for lower index values ($n \in [1.25, 3.0]$) the achievable V_{r0} is strongly dependent on the refractive index, showing a $1/n^7$ -scaling across part of this interval. It is seen that given a refractive index corresponding to a polymer ($n \approx 1.25$) it is not found to be possible to achieve $V_{r0} < 1[\lambda/(2n_{\text{InP}})]^3$, limiting the utility of polymer-based 3D printing for realizing the studied devices. Further, it is seen that as n increases beyond $n = 3.5$ the reduction of V_{r0} flattens out, suggesting that once the index contrast between the background and the dielectric becomes sufficiently large the effect on the attainable V_{r0} tapers off.

The second study concerns the effect of the allowable device volume on V_{r0} (see Fig. 5b). Here $n = 3.5$ and a central feature width of 8 nm are chosen as fixed parameters. Three device volumes are

considered, namely $V \approx \{0.5, 2.2, 6.7\}[\lambda]^3$. Remarkably, the overall allowable device volume is seen to only have a limited effect on the attainable V_{r0} , only reducing by approximately 25% as the device volume increases by more than an order of magnitude.

The third and final study concerns the effect of the central feature width w , the results of which are presented in Fig. 5c. Here $n = 3.5$ and a device volume of approximately $2[\lambda]^3$ are used. From the panel a scaling of $w^{4/3}$ is observed, revealing that until the assumed physics model breaks down, as the central feature approaches atomic scale, the mode volume decreases with bridge width, approaching $V_{r0} = 10^{-4}[\lambda/(2n)]^3$ as w approaches 0.1 nm.

In this work we have studied how 3D-sculpting the electromagnetic environment affects the minimum achievable single-emitter mode volume in dielectric structures. We have found that single-emitter mode

volumes more than three(four) orders of magnitude below the diffraction limit can be achieved for material(air) confinement. This constitutes a reduction of between one and two orders of magnitude compared to the 2D-patterned planar counterparts proposed in recent literature. Further, we show that by introducing a set of carefully designed ellipsoidal shells, and a connecting rod for mechanical feasibility, it is possible to increase the spectral confinement by many orders of magnitude ($Q > 10^8$ demonstrated numerically), thus revealing a path to systematically and individually tailor both Q and V_{r_0} for particular ap-

plications. Given advances in nano-scale fabrication technology, the devices envisioned in this work holds the potential for enabling light-matter interaction at unprecedented strengths in near-lossless dielectric environments. We expect experimental investigation and exploitation of the proposed geometries in the microwave regime, using existing 3D-printing tools in the immediate future.

The authors thank Olav Breinbjerg for helpful discussions and the Danish National Research Foundation for funding through grant DNRF147, NanoPhoton.

-
- [1] E. M. Purcell, Spontaneous emission probabilities at radio frequencies, *Physical Review* **69**, 681 (1946).
- [2] M. Notomi, Manipulating light with strongly modulated photonic crystals, *Reports on Progress in Physics* **73(9)**, 096501 (2010).
- [3] X. Ding, Y. He, Z.-C. Duan, N. Gregersen, M.-C. Chen, S. Unsleber, S. Maier, C. Schneider, M. Kamp, S. Höfling, C.-Y. Lu, and J.-W. Pan, On-demand single photons with high extraction efficiency and near-unity indistinguishability from a resonantly driven quantum dot in a micropillar, *Physical Review Letters* **116(2)**, 020401 (2016).
- [4] Y. Yamamoto, S. Machida, and G. Björk, Microcavity semiconductor laser with enhanced spontaneous emission, *Physical Review A* **44**, 657 (1991).
- [5] E. K. Lau, A. Lakhani, R. S. Tucker, and M. C. Wu, Enhanced modulation bandwidth of nanocavity light emitting devices, *Optics Express* **17(10)**, 7790 (2009).
- [6] T. Suhr, N. Gregersen, K. Yvind, and J. Mørk, Modulation response of nanoleds and nanolasers exploiting purcell enhanced spontaneous emission, *Optics Express* **18(11)**, 11230–11241 (2010).
- [7] J. Khurgin, How to deal with the loss in plasmonics and metamaterials, *Nature Nanotechnology* **10**, 2 (2015).
- [8] J. T. Robinson, C. Manolatou, L. Chen, and M. Lipson, Ultrasmall mode volumes in dielectric optical microcavities, *Physical Review Letters* **95**, 143901 (2005).
- [9] A. Gondarenko, S. Preble, J. Robinson, L. Chen, H. Lipson, and M. Lipson, Spontaneous emergence of periodic patterns in a biologically inspired simulation of photonic structures, *Physical Review Letters* **96**, 143904 (2006).
- [10] X. Liang and S. G. Johnson, Formulation for scalable optimization of microcavities via the frequency-averaged local density of states, *Optics Express* **21**, 30812–30841 (2013).
- [11] H. Choi, M. Heuck, and D. Englund, Self-similarnanocavity design with ultrasmall modevolume for single-photon nonlinearities, *Physical Review Letters* **118(22)**, 223605 (2017).
- [12] S. Hu, M. Khater, R. Salas-Montiel, E. Kratschmer, S. Engelmann, W. M. J. Green, and S. M. Weiss, Experimental realization of deep-subwavelength confinement in dielectric optical resonators, *Science Advances* **4(8)**, eaat2355 (2018).
- [13] F. Wang, R. E. Christiansen, Y. Yu, J. Mørk, and O. Sigmund, Maximizing the quality factor to mode volume ratio for ultra-small photonic crystal cavities, *Applied Physics Letters* **113**, 241101 (2018).
- [14] S. Mignuzzi, S. Vezzoli, S. A. R. Horsley, W. L. Barnes, S. A. Maier, and R. Sapienza, Nanoscale design of the local density of optical states, *Nano Letters* **19**, 1613 (2019).
- [15] G. Isiklar, P. T. Kristensen, J. Mørk, O. Sigmund, and R. E. Christiansen, On the trade-off between mode volume and quality factor in nanocavities optimized for purcell enhancement, *Optics Express* **30(26)**, 47304 (2022).
- [16] M. Albrechtsen, B. V. Lahijani, R. E. Christiansen, V. T. H. Nguyen, L. N. Casses, S. E. Hansen, N. Stenger, O. Sigmund, H. Jansen, J. Mørk, and S. Stobbe, Nanometer-scale photon confinement in topology-optimized dielectric cavities, *Nature Communications* **13**, 6281 (2022).
- [17] M. Xiong, R. E. Christiansen, F. Schröder, Y. Yu, L. N. Casses, E. Semanova, K. Yvind, N. Stenger, O. Sigmund, and J. Mørk, Experimental realization of deep sub-wavelength confinement of light in a topology-optimized inp nanocavity, *Optical Materials Express* (**Accepted**) (2024).
- [18] A. Grigorescu and C. Hagen, Resists for sub-20-nm electron beam lithography with a focus on hsq: state of the art, *Nanotechnology* **20**, 292001 (2009).
- [19] J. Y. E. Chan, Q. Ruan, M. Jiang, H. Wang, H. Wang, W. Zhang, C.-W. Qiu, and J. K. W. Yang, High-resolution light field prints by nanoscale 3d printing, *Nature Communications* **12**, 3728 (2021).
- [20] R. L. Truby and J. A. Lewis, Printing soft matter in three dimensions, *Nature* **540**, 371 (2016).
- [21] D. Oran, S. G. Rodrigues, R. Gao, S. Asano, M. A. Skylar-Scott, F. Chen, P. Tillberg, A. Marblestone, and E. S. Boyden, 3d nanofabrication by volumetric deposition and controlled shrinkage of patterned scaffolds, *Science* **362(6420)**, 1281–1285 (2018).
- [22] D. Zhao, A. Han, and M. Qiu, Ice lithography for 3d nanofabrication, *Science Bulletin* **64**, 865 (2019).
- [23] R. Levi-Setti, Proton scanning microscopy: feasibility

- ity and promise, *Scanning Electron Microscopy* 1974, 125 (1974).
- [24] A. N. Babar, T. A. S. Weis, K. Tsoukalas, S. Kadkhodazadeh, G. Arregui, B. V. Lahijani, and S. Stobbe, Self-assembled photonic cavities with atomic-scale confinement, *Nature* **624**, 57 (2023).
- [25] M. P. Bense and N. Kikuchi, Generation of optimal topologies in structural design using a homogenization method, *Computer Methods in Applied Mechanics and Engineering* **71**, 197 (1988).
- [26] R. E. Christiansen and O. Sigmund, Inverse design in photonics by topology optimization: tutorial, *Journal of the Optical Society of America B* **38**, 496 (2021).
- [27] S. Molesky, Z. Lin, A. Y. Piggott, W. Jin, J. Vuckovic, and A. W. Rodriguez, Inverse design in nanophotonics, *Nature Photonics* **12**, 659 (2018).
- [28] J. S. Jensen and O. Sigmund, Topology optimization for nano-photonics, *Laser & Photonics Reviews* **5**, 308 (2011).
- [29] P. T. Kristensen, C. V. Vlack, and S. Hughes, Generalized effective mode volume for leaky optical cavities, *Optics Letters* **37**(10), 1649 (2012).
- [30] J. Jin, *The Finite Element Method in Electromagnetics* (Wiley-Interscience, 2013).
- [31] K. Svanberg, A class of globally convergent optimization methods based on conservative convex separable approximations, *SIAM Journal on Optimization* **12**(2), 555 (2002).
- [32] Comsol multiphysics® v. 6.1, www.comsol.com/comsol-ab, .
- [33] M. Zhou, B. S. Lazarov, and O. Sigmund, Topology optimization for optical projection lithography with manufacturing uncertainties, *Applied Optics* **53**, 2720 (2014).
- [34] F. Wang, B. S. Lazarov, and O. Sigmund, On projection methods, convergence and robust formulations in topology optimization, *Structural Multidisciplinary Optimization* **43**, 767 (2011).
- [35] M. Albrechtsen, B. V. Lahijani, and S. Stobbe, Two regimes of confinement in photonic nanocavities: bulk confinement versus lightning rods, *Optics Express* **30**(9), 15458 (2022).
- [36] J. Mork and G. L. Lippi, Rate equation description of quantum noise in nanolasers with few emitters, *Applied Physics Letters* **112**(14), 141103 (2018).